JOURNAL OF SPACECRAFT AND ROCKETS
Vol. 29, No. 3, May-June 1992

Predicted Flight Performance of Base-Bleed Projectiles

James E. Danberg* and Charles J. Nietubicz*
U.S. Army Ballistic Research Laboratory, Aberdeen Proving Ground, Maryland 21005

Current Army programs are applying a base-bleed concept to achieve increased range for projectiles. Base bleed is a technique in which low-speed mass is injected into the base region to reduce base drag and extend range. The U.S. Army Ballistic Research Laboratory is developing an engineering computational model capable of predicting the flight performance. The model analyzes three problem elements: a solid propellant gas generator, the effect of injection on the aerodynamic drag, and trajectory computations. Because each element is time dependent, all three must be solved simultaneously. The analysis is based on experimental and numerical data generated for the M864 base-bleed projectile. Navier-Stokes computations for the near wake region have been performed on the Army's Cray X-MP/48 supercomputer. The results were used to correlate base pressure change with injection rate, gas temperature, and Mach number. These results provide critical data for the analysis. The mass generation analysis is combined with the effect of mass injection on base pressure to obtain the projectile base drag at each step of a two-dimensional, point-mass trajectory computation. Computed results are in reasonable agreement with the flight data. Ranges are predicted within 4.2%.

Nomenclature

A	= area
C_v	= discharge coefficient
$\hat{E}$, $\hat{G}$, $\hat{H}$	= flux vectors
I	= injection parameter
K	= constant, see Eq. (3)
M	= Mach number
$\dot{m}$	= mass flow
P	= pressure
$\hat{q}$	= vector of dependent variables
Re	= Reynolds number
$\dot{r}$	= regression rate
$\hat{S}$	= viscous source vector
T_0	= stagnation temperature
u, v, w	= Cartesian velocity components
γ	= ratio of specific heats
ζ, ξ	= transformed spatial variables
ρ_s	= propellant density
τ	= time

Subscripts

b	= base
c	= cylindrical
j	= exit
s	= slot
sl	= sea level
∞	= freestream

Introduction

The addition of gas into the near wake at low speed (in contrast with rocket propulsion) is an effective means of reducing drag and increasing the range of artillery projectiles. This technique is termed base bleed in the following because nonreacting mass transfer is considered. The term base burn is reserved for the case of combustion in the wake.

The primary objective of this work is the development of an engineering analysis model for base-bleed projectile flight performance. A schematic of the M864 including the base-bleed propellant in the afterbody is shown in Fig. 1. The engineering model considers all three elements of the problem, namely, gas generation, effect of bleed on aerodynamic drag, and a trajectory model. Because each of these elements is time dependent, all three elements must be solved simultaneously. This is in contrast with the conventional projectile where the aerodynamic coefficients are typically determined independent of any specific trajectory. The analysis will be based on much of the existing experimental and numerical data obtained as part of the M864 program. However, the techniques developed are easily adapted to other designs.

A secondary objective is to determine how the numerical solutions to the Navier-Stokes equations can be applied to the problem. At present these computations do not account for the time-dependent nature or real-gas properties of the gas generator and the changing freestream conditions along the trajectory. Thus, steady-state solutions are obtained for specific freestream conditions with equivalent air mass flow and temperature imposed as boundary conditions at the exit of the gas generator. The results of these computations are used for correlations of base pressure as a function of injected mass flow and temperature.

Gas Generator

The M864 gas generator is housed in the boattail afterbody. It consists of two identical solid propellant grains. These grains provide an inner cylindrical burning surface and four planar surfaces separated by a 3-mm slot. Miller and Holmes[1] measured the propellant burning rate over a range of subatmospheric pressures using a strand-burning technique. The strand-burning rate $\dot{r}_0$ was found to be $\dot{r}_0 = 0.00009132\ P_c^{0.6655}$ where P_c is in bars and $\dot{r}_0$ is in m/s. The burning rate on the cylindrical surface of M864 propellant $\dot{r}_c$ and on the slot surface $\dot{r}_s$ are considered uniform over the surfaces but may possibly be different. Thus the mass generated by the solid propellant can be written as follows:

$$\dot{m} = \rho_s(\dot{r}_c A_c + \dot{r}_s A_s) \tag{1}$$

Ground-Based Spin Fixture

Gas generator tests have been performed where an actual M864 gas generator was mounted on a spin fixture.[2] Chamber temperature, chamber pressure, and burn time were measured for various rates of spin. The chamber pressure measurement

Presented as Paper 90-2069 at the AIAA/ASME/SAE/ASEE 26th Joint Propulsion Conference, Orlando, FL, July 16-18, 1990; received June 15, 1990; revision received June 8, 1991; accepted for publication Aug. 29, 1991.

*Aerospace Engineer. Associate Fellow AIAA.

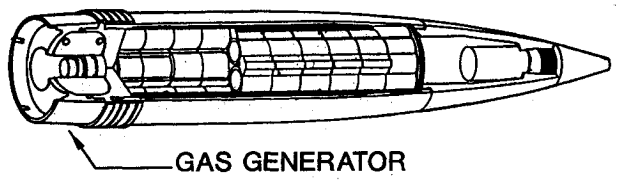

Fig. 1 Schematic of M864.

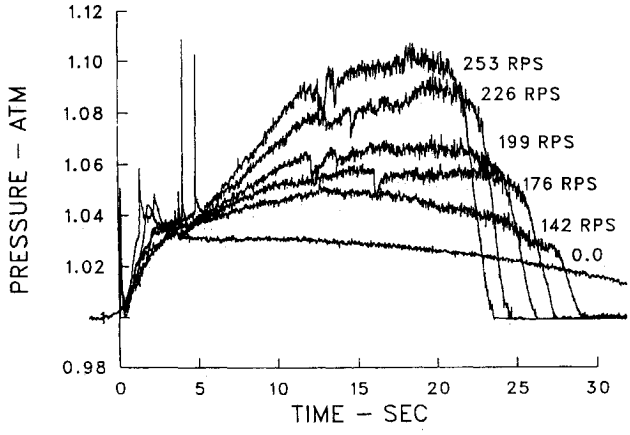

Fig. 2 Measured chamber pressures.[2]

is shown in Fig. 2. The measured chamber pressure-time histories can be interpreted as indicating that there is a difference between the burning rate on the cylindrical surface and on the surface of the slot. The chamber pressure is directly an indication of the exit mass flow. If the burning rates are equal on the two surfaces, then the chamber pressure should decrease monotonically with time, after an initial transient because of the shape of the grains. As shown in Fig. 2, at high spin rates the pressure initially increases and then falls off, indicating that the cylindrical surface is more important in determining the mass flow, and thus chamber pressure, than the monotonically varying slot contribution.

The mass flow $\dot{m}$, is assumed subsonic but described by the following compressible flow equation:

$$\dot{m} = K\sqrt{\frac{\gamma}{(\gamma-1)}\left[\left(\frac{P_c}{P_b}\right)^{(\gamma-1)/\gamma} - 1\right]} \tag{2}$$

where P_c is the chamber pressure, P_b is the external pressure, and γ is the ratio of specific heats of the exhaust products ($\gamma = 1.25$). The factor K can be written

$$K \equiv C_v A_j \sqrt{2\rho_j P_b} \tag{3}$$

where C_v, A_j, and ρ_j are the discharge coefficient, exit area, and exit density, respectively. Since each is approximately constant, K may also be taken as constant in these laboratory tests. In the zero-spin case, the regression rates are presumed to be the same on both surfaces, and approximately equal to the strand burning $\dot{r}_0$, since the chamber pressure history is basically monotonically decreasing with time. The zero-spin chamber pressure distribution can be used to determine the constant K, which according to data of Kayser et al.[2] gives $K = 0.189$ kg/s.

Effect of Spin

When spinning, the cylindrical and slot surfaces are assumed to have different regression rates that are determined as follows. The radial thickness of the grain is the smallest dimension and thus the total burn time determines the burn rate on the cylindrical surface. The mass flow, Eq. (1), is integrated over time for the known amount of propellant using different $\dot{r}_c$ values until the calculated burn time matches the measured time.

Next, it is observed (see Fig. 2) that there is an initial transient that is relatively independent of spin. The pressure is 3.3% higher than ambient at 3.3 s after ignition for all spin rates. After that point, the chamber pressures diverge, depending on spin. The regression rates were computed during the initial transient phase, assuming they were identical but time varying.

Finally the slot contribution affects the magnitude of $\dot{m}$, but it does not affect the burnout time. Conditions at the end of the initial transient phase define the burning rate of the slots. This is equivalent to assuming that the mass flux from the gas generator is independent of spin at the end of the initial transient phase.

The results are shown in Fig. 3 where the predicted chamber pressure is plotted against time for the various spin rates of the spin fixture tests. This figure can be compared with Fig. 2. Very good agreement is obtained, particularly during the early period, when the effect of the different spin rates is being observed. The most important result, for subsequent calculations of the flight case, is Fig. 4, which shows $\dot{r}_c$ and $\dot{r}_s$ normalized by the strand-burning rate as a function of spin.

Application to Flight Test

In applying the previous analysis to the flight situation, it is assumed that the exit pressure P_b becomes the base pressure and

$$K_{\text{flight}} = K\frac{P_b}{P_{sl}} \tag{4}$$

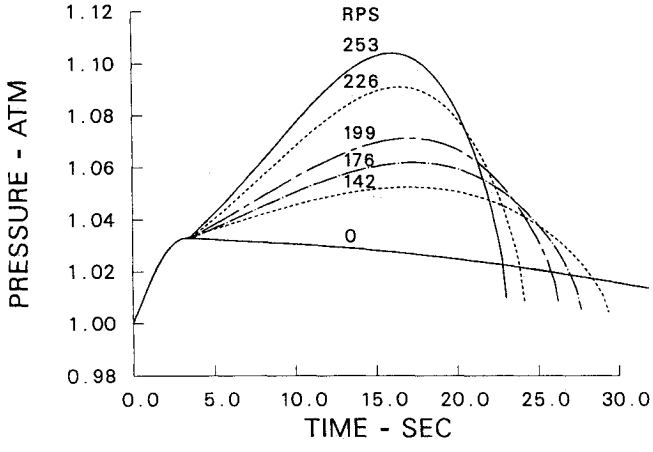

Fig. 3 Computed chamber pressures.

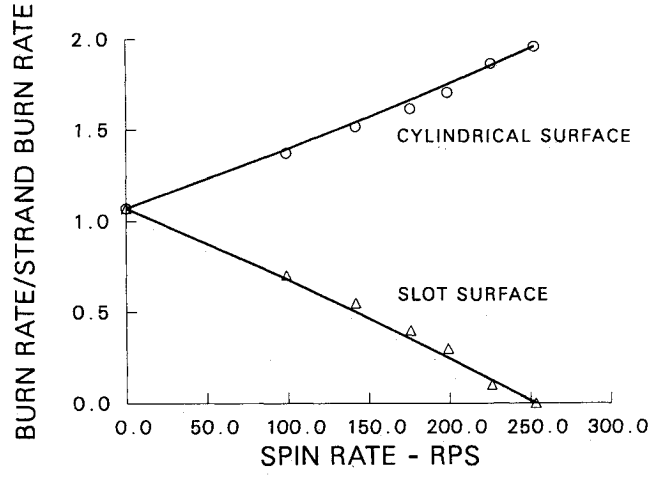

Fig. 4 Effect of spin rate on burn rate.

where P_{sl} is sea level pressure. The mass flow generation formula, Eq. (1), remains the same. Equations (1) and (2) may be considered, at each point in time, as two equations with four unknowns: $\dot{m}$, P_b/P_∞, P_c/P_∞, and P_∞/P_{sl}. Along the trajectory, M_∞ and P_∞/P_{sl} would be known, and aerodynamic theory gives a third relation between $\dot{m}$ and P_b/P_{sl} (also involving M_∞ and P_∞/P_{sl}) that determines the solution at each point in time.

The solid propellant fuel is relatively difficult to ignite, and therefore the gun gases are supplemented by an igniter that consists of two 6.2-g cylindrical pellets of magnesium Teflon. The igniter is consumed in 2 s and contributes significantly to the mass flow in the first seconds of flight.

Aerodynamics of Base Injection

It is customary when considering base-bleed or burn to define a nondimensional injection parameter I:

$$I = \frac{\dot{m}}{\rho_\infty u_\infty A_b} \tag{5}$$

In the M864 case, the average value of this parameter is about 0.002 at launch and increases with decreasing Mach number and increasing altitude.

Most supersonic wind-tunnel experiments on this subject are concerned with cold gas injection into the base region at relatively large values of I. Figure 5 shows the results of one such experiment by Kayser.[3] He investigated the effect of the injector geometry (i.e, percent open area of the base) on the base pressure. The results are for a Mach number of 3.0 with cold air injected into the model wake. Note that there is a strong dependence on injector open area at large values of I. However, all of the curves originate at the same pressure and increase linearly at the same slope for values of I less than 0.005. This suggests that, at small injection rates, a linear increase in base pressure can be assumed, although as the injection rate gets larger such an approximation may overestimate the beneficial effects.

Linear Effect of Injection on Base Pressure

As an engineering approach, it is assumed that the mass injection rate is at sufficiently low subsonic velocities that the injection effect on base pressure is nearly linear, i.e.,

$$\frac{P_b}{P_\infty} = \left(\frac{P_b}{P_\infty}\right)_{I=0} + \left[\frac{\mathrm{d}(P_b/P_\infty)}{\mathrm{d}I}\right]_{I=0} I \tag{6}$$

A number of reports on wind-tunnel measurements of base pressure with injection have been examined. Figure 6 shows the results of determining $[\mathrm{d}(P_b/P_\infty)/\mathrm{d}I]_{I=0}$ as a function of the freestream Mach number. The open symbols represent a

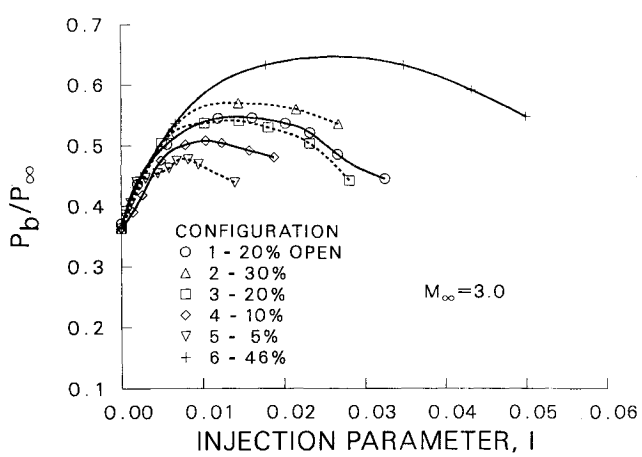

Fig. 5 Measured[3] base presssures vs I.

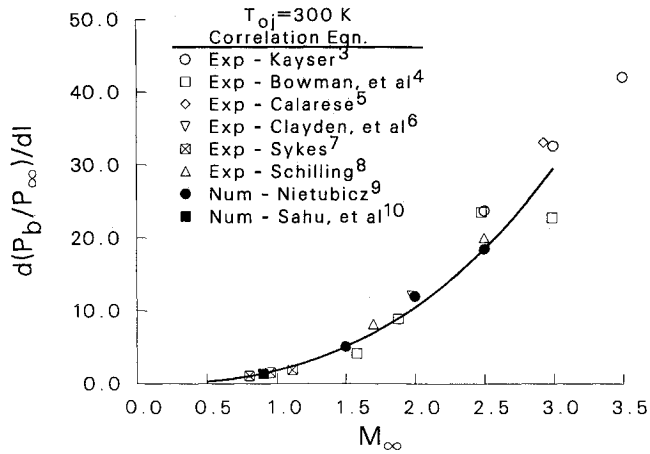

Fig. 6 Correlation of slope of base pressure vs I, T_{0j} = 300 K.

number of wind-tunnel experiments[3-8] in which ambient room temperature air was injected. Although these data correlate reasonably well with Mach number, they represent a special case of low-temperature injection into a low temperature wake. (Stagnation temperature of the wind-tunnel flow is estimated also to be ambient room temperature.) Also included in Fig. 6 are four points (filled symbols) computed by Nietubicz and Sahu[9] and Sahu et al.[10] The magnitude of the numerical results agrees quite well with the wind-tunnel data.

Other numerical computations[9] of the near wake flow with injection have been performed to broaden our data base for these kinds of flows. These computations, which involve solution of the perfect gas Navier-Stokes equations, are discussed in the following sections.

Navier-Stokes Computational Technique

The time-dependent, thin-layer, Navier-Stokes equations are solved numerically to obtain a solution to this problem. The numerical technique used is an implicit finite difference scheme. The steady flow, which is the desired result, is obtained in a time asymptotic fashion. The time-dependent, thin-layer, Navier-Stokes equations written in strong conservation law form for the axisymmetric formulation[11] are

$$\frac{\partial \hat{q}}{\partial \tau} + \frac{\partial \hat{E}}{\partial \xi} + \frac{\partial \hat{G}}{\partial \zeta} + \hat{H} = \frac{1}{Re}\frac{\partial \hat{S}}{\partial \zeta} \tag{7}$$

The general coordinate transformations are defined as follows: $\xi = \xi(x,y,z)$ is the longitudinal coordinate, $\zeta = \zeta(x,y,z)$ is the near normal coordinate, and $\tau = t$ is the time.

The vector $\hat{q}$ contains the dependent variables $[\rho, \rho u, \rho v, \rho w, e]$, and the flux vectors $\hat{E}$ and $\hat{G}$ contain terms that arise from the conservation of mass, momentum, and energy. The source vector $\hat{H}$ in Eq. (7) contains terms that result from an analytic determination of the circumferential flux vector given the assumption of axisymmetric flow and constant angular velocity.[11] The viscous terms are contained in the vector $\hat{S}$ that is seen to have variation in the ζ direction only. This is representative of the thin-layer approximation.

The numerical algorithm used for the solution of Eq. (7) is the Beam and Warming[12] implicit, approximately factored, finite difference scheme that uses central differencing in both ξ and ζ directions. Code improvements have been made to include a variable time step, numerical smoothing based on local solution gradients, and code vectorization.[13] The Beam-Warming implicit algorithm has been used in various applications for the equations in general curvilinear coordinates. The algorithm is first-order accurate in time and second- or fourth-order accurate in space. Central difference operators are employed; the algorithm produces a block tridiagonal system for each space coordinate. The main computational work is con-

tained in the solution of these block tridiagonal systems of equations.

The axisymmetric code that solves Eq. (7) uses a unique flowfield segmentation procedure to compute the full flowfield over a projectile or a missile, including the base region. Although the thin-layer approximation is not valid in the wake region, this segmentation procedure allows for turbulent quantities to be determined across the shear layer.[14] This has provided reasonable accuracy for supersonic flows. For the computation of turbulent flows, the two-layer algebraic, Baldwin-Lomax,[15] turbulence model is used over the projectile body.

The solution time for the unsteady Navier-Stokes code is primarily dependent on the convergence time for the subsonic equations of the base region and nose region flowfield. The supersonic portion over the body converges within 700 time steps. Although a space-marching technique could be used for the supersonic region, it would not yield a significant overall time savings.

Boundary Conditions

The outer computational boundary where freestream conditions were imposed was kept at approximately 12 body diameters from the body surface. At the downstream boundary, extrapolated outflow conditions were used. Viscous no-slip boundary conditions were imposed on all solid surfaces. The normal momentum equation was solved at the wall for p_n, the normal pressure gradient. The free-flight wall temperature is specified. Using the time-lagged pressure, the density at the wall is determined.

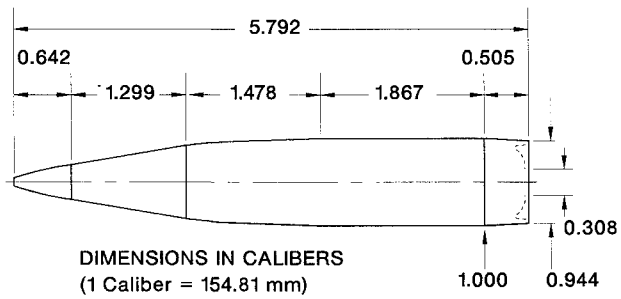

Fig. 7 Computational model.

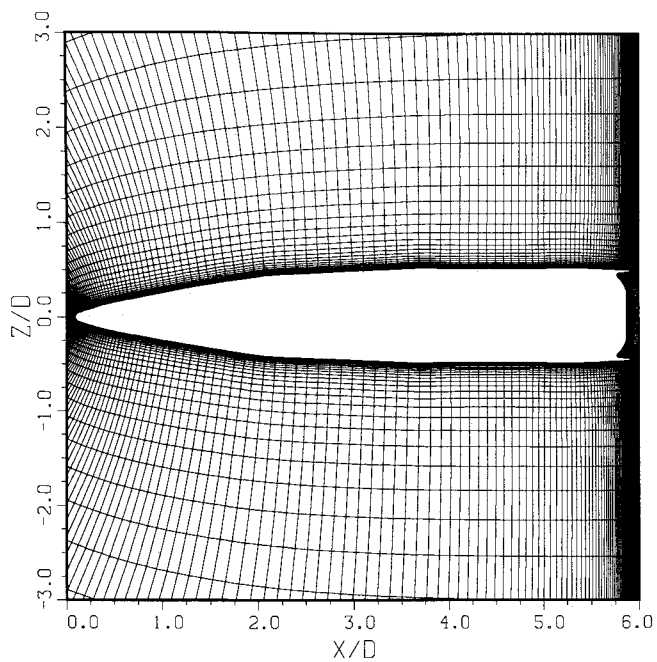

Fig. 8 Grid near the model.

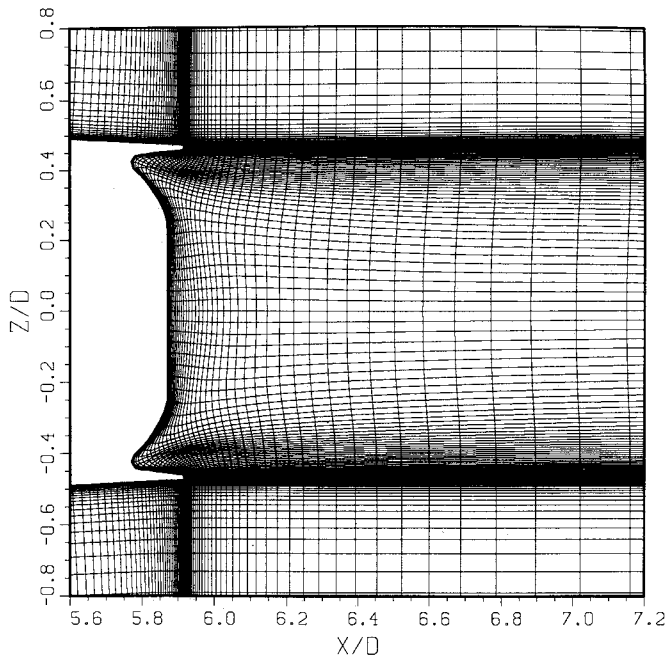

Fig. 9 M864 dome base grid.

The boundary conditions on the exit of the gas generator follow from the computed pressure and flowfield variables at each time step. The bleed boundary conditions are thus lagged in time. The bleed conditions $(\rho u)_j$ and T_{0_j} are specified whereas p_j at the gas generator exit is extrapolated from the exterior flow. By specifying the mass injection rate I, the bleed Mach number M_j can be directly solved by

$$M_j^2 = \frac{1}{\gamma - 1}\left\{-1 + \sqrt{1 + 2(\gamma - 1)\frac{T_{0_j}}{T_\infty}\left[IM_\infty \frac{P_\infty A_b}{P_j A_j}\right]^2}\right\} \tag{8}$$

where A_b and A_j are the area of the base and bleed opening, respectively. Using isentropic relations, the bleed stagnation pressure p_{0_j} and static temperature T_j can be calculated. Given the temperature and pressure, the density is computed and the boundary conditions for the next time step are obtained.

Model Geometry and Computational Grid

The computational model of the M864 is shown in Fig. 7. Projectile features that have not been modeled exactly are the fuse meplat and the rotating band. The rotating band was eliminated and the meplat was modeled as a hemisphere cap. The model nose is a combination of ogive and conical sections. The cylindrical section is slightly undercut, and the boattail length is 0.505 calibers with a 3-deg angle. The shape of the base is shown as a dotted line on the boattail. The base burn motor is located internally with the exhaust port centered on the model axis.

Figure 8 shows the computational grid generated over the projectile body including the base. It consists of 265 longitudinal points and 60 points in the normal direction. This is broken down into two sections: a body region and a base region. The surface points for each region are selected using an interactive design program. Each grid section is then computed separately using a hyperbolic grid generation program.[16] Figure 9 shows an expanded view for the dome base grid. The configuration for the concave dome base required an increase in the smoothing values used by the hyperbolic grid generator as well as the addition of a grid cell averaging technique.

Computational Results and Correlation

Computations have been performed for the M864 dome base with the inclusion of base bleed. The computations to

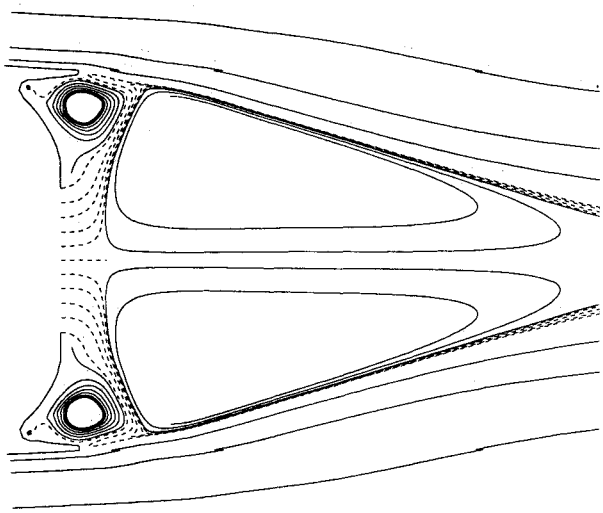

Fig. 10 Particle traces, $M_\infty = 2.0$, $T_{0j} = 300$ K.

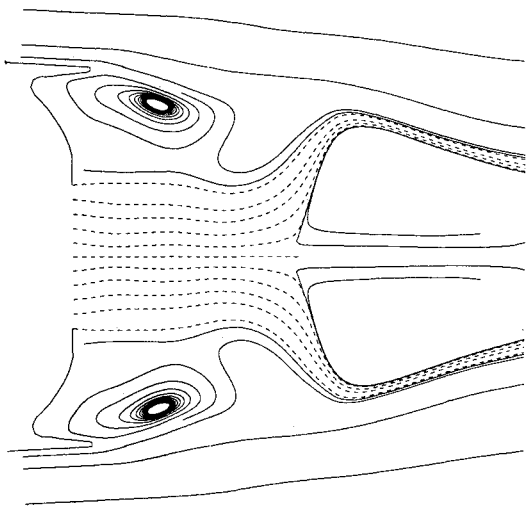

Fig. 11 Particle traces, $M_\infty = 2.0$, $T_{0j} = 1200$ K.

date have been for cold and hot mass flow, with values of the mass injection parameter I up to 0.04. Although the actual mass flow rate varies over the course of the trajectory, the present calculations were run to see the effect on drag across a Mach number range.

As an attempt to model the effects of burning, computations were run with hot mass addition. The results shown in Figs. 10 and 11 are particle traces in the base region for bleed gas temperatures of 300 and 1200 K, respectively. The dashed traces are particles that originate from the bleed ejection hole. The solid traces were released in various parts of the flowfield. The effect of temperature is rather dramatic in changing the recirculation pattern within the base flowfield. At the lower temperature, the bleed gas is shown to be captured by the recirculation region near the base. As the temperature is increased, all of the bleed gas moves downstream. The higher temperature gives rise to an increased velocity and thus an effective increase in the mass injection parameter.

The results of these computations, in terms of the linear effect of injection, are shown in Fig. 12. The data are unique in that they illustrate the combined effect of Mach number and injected gas temperature. The computed data at an injection temperature of 1500 K are consistent with the only data available.[17] At all stagnation temperatures of the gas, the slope $[\mathrm{d}(P_b/P_\infty)/\mathrm{d}I]_{I=0}$ increases rapidly with Mach number and almost linearly with temperature. An approximate formula that describes the data is

$$\left[\frac{\mathrm{d}(P_b/P_\infty)}{\mathrm{d}I}\right]_{I=0} = (-5.3953 + 0.01723T_{0j})M_\infty + (4.6101 - 0.01463T_{0j})M_\infty^2 + (-0.5660 + 0.00446T_{0j})M_\infty^3 \quad (9)$$

Note that with this linear model of base pressure vs injection rate (Eq. 6), it is possible to correct the no injection base drag to account for base bleed. At each step in a trajectory calculation where an estimate of Mach number, freestream static pressure, spin rate, and inert (no-injection) drag coefficients are specified, then Eqs. (1), (2), (4), and (5) can be solved simultaneously to find the change in base pressure with injection.

Results

The theory described in the previous sections has been used to develop a computer program that includes a two-dimensional, modified point mass trajectory model based on the work of Lieske and Reiter.[18] The resultant technique has been compared with several flight test cases. The primary case is that of an instrumented[19] M864 in which the base and combustion chamber pressures were measured in flight. Radar data also have been obtained by Lieske[20] over a range of launch conditions. These results are compared with the present model's predictions.

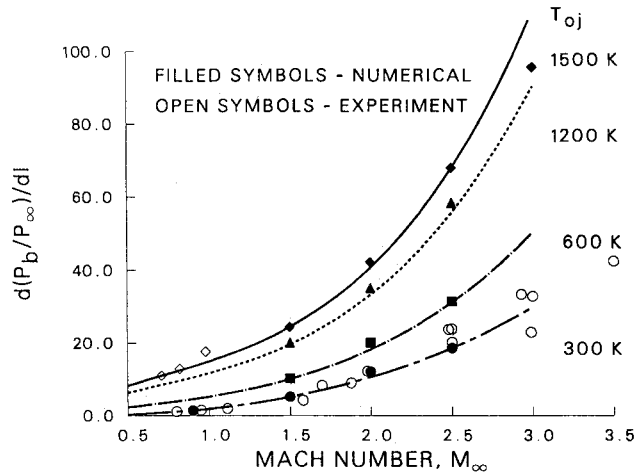

Fig. 12 Correlation of slope of base pressure vs I, $T_{0j} \geq 300$ K.

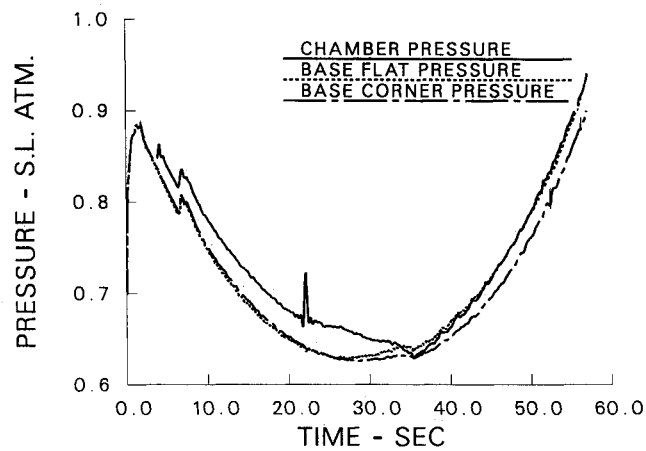

Fig. 13 Pressures measured[19] in flight.

Instrumented Flight Test Case

Kayser et al.[19] launched an instrumented M864 in September 1988. The projectile contained pressure transducers to monitor the static pressure at two points on the base and the stagnation pressure in the combustion chamber. In addition, a thermocouple measured the temperature in the combustion chamber. These data were telemetered to recording stations on the ground. The projectile was not a standard M864 in that the mass was 81.9% of normal. The launch conditions were Mach 1.30 at a gun elevation of 47.8 deg.

Figure 13 shows the main result of the experiment, which is the pressure-time histories for two points on the base and in the chamber. The origin of the time scale is with respect to the exit of the shell from the gun. The initial base pressure corresponds to the inert projectile at Mach number of 1.30. The two base pressure taps indicated almost the same pressure throughout the burning phase, although there was a significant difference after burnout. A significant pressure jump was observed as the projectile decelerates through Mach 1 at 8-9 s into the flight. The chamber pressure measurements roughly parallel the base pressures but at a somewhat higher level as needed to produce the gas generator exhaust.

Figure 14 shows the computed pressure histories using the present analysis. The results are in reasonably good accord with the previous experimental data. There are some discrepancies, including the fact that the base pressure did not jump up as high initially. This would seem to indicate that the initial drag reduction is not as great as obtained in flight. A third line on this figure indicates the local ambient static pressure along the trajectory. The base pressure actually becomes larger than the local static pressure, indicating a thrust is being generated near the apogee. The chamber pressure history also roughly parallels the base pressure. The burnout is clearly observed at 36.8 s.

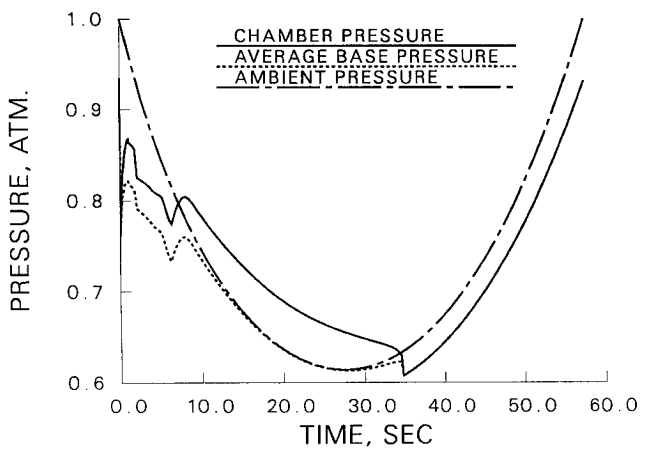

Fig. 14 Computed pressures.

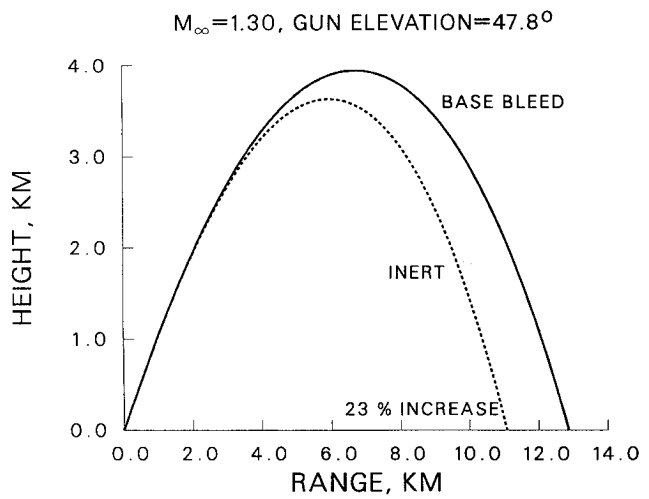

Fig. 15 Predicted M864-L trajectories.

Table 1 Predicted flight range data for M864

Launch Mach no.	Gun elevation = 47.8 deg: Range computed, km	Range from firing tables, km	Δ, %
1.30	12.8	12.6	+2.0
1.61	17.9	17.2	+4.2
1.97	22.2	22.0	+1.1
2.37	27.3	28.1	−2.9

Figure 15 shows a comparison between the predicted trajectory for this round with the motor on and with motor off. The effect of drag reduction caused by the gas generator results in a 23% increase in range.

Comparison with Firing Table Data

To develop firing information for the M864, the U.S. Army Ballistic Research Laboratory has been conducting flight tests of production ammunition over a wide range of conditions. The flight experiments employ Doppler radar to track the trajectory. From these measurements and three-dimensional modified point mass simulation, the drag and velocity of the projectile in flight are deduced. The data reduction technique and results have been reported by Lieske.[20] The modeling analysis developed here has been applied to some of these cases. A picture of the ability of the model to predict M864 flight performance can be obtained from Table 1 in which the range as determined by firing tables is compared with the current model. The table also includes a fourth case of the lightweight projectile launched with a nonstandard charge. This table shows that the computation gives the correct trend and magnitude. The present model agrees with that predicted by firing tables computation within 800 m for the four cases considered.

Concluding Summary

An engineering model for the performance of the M864 base burn projectile has been assembled and tested on a number of flight cases. The model takes into account the three main elements of the problem: a gas generator mass flow prediction, the drag reduction caused by the mass injected into the wake, and a two-dimensional modified point mass trajectory computation. This new predictive capability provides qualitative predictions of all of the physical aspects of the system's performance. The computer model is based on laboratory experiments, analysis, and flight tests of the inert shell. No special factors have been introduced to improve the agreement with measured data from flights of the M864 projectile.

The Navier-Stokes computations of the base flow have been a critical element in formulating a comprehensive model. These computations have been used to provide a correlation of change in base pressure with mass injection and Mach number and taking into account the temperature of the gas. This later effect is of critical importance for the development of a physically realistic model of the effect of mass addition on drag reduction. Applicable data have been unavailable in previous experimental studies.

The M864 analytical model has been compared with an instrumented flight case. The chamber pressure and base pressure vs time are successfully predicted. The burnout time predicted was 36.8 s compared with an observed burnout of 35.3 s. Time of flight is also predicted within 1 s. The model was also applied to a number of normal operational flight conditions. Correct trends and range values within 4.2% of those from Doppler radar were obtained.

The developed engineering model provides a significant new tool for the analysis of future designs. Current programs in

extended range artillery are using this analysis for initial design guidance.

References

[1]Miller, M. S., and Holmes, H. E., "Subatmospheric Burning Rates and Critical Diameters for AP/HTPB Propellant," *Journal of Propulsion and Power,* Vol. 6, No. 5, 1990, pp. 671,672.

[2]Kayser, L. D., Kuzan, J. D., and Vazquez, D. N., "Ground Testing for Base-Burn Projectile Systems," U. S. Army Ballistic Research Lab., BRL-MR-3708, AD A201107, Aberdeen Proving Ground, MD, Nov. 1988.

[3]Kayser, L. D., "Effects of Base Bleed and Supersonic Nozzle Injection on Base Pressure," U.S. Army Ballistic Research Lab., Memorandum Rept. 2456, AD B003442L, Aberdeen Proving Ground, MD, March 1975.

[4]Bowman, J. E., and Clayden, W. A., "Cylindrical Afterbodies in Supersonic Flow with Gas Ejection," *AIAA Journal,* Vol. 5, No. 8, 1967, pp. 1524,1525.

[5]Calarese, W., "GAU-8 Projectile Afterbody Drag Reduction by Boattailing and Base Injection with Heat Addition," AIAA Paper 79-0146, Jan. 1979.

[6]Clayden, W. A., and Bowman, J. E., "Cylindrical Afterbodies at $M_\infty = 2$ with Hot Gas Ejection," *AIAA Journal,* Vol. 6, No. 12, 1968, pp. 2429-2431.

[7]Sykes, D. M., "Cylindrical and Boattailed Afterbodies in Transonic Flow with Gas Ejection," *AIAA Journal,* Vol. 8, No. 3, 1970, pp. 588,589.

[8]Schilling, H., "Experimental Investigation on the Base-Bleed-Effect for Body-Tail Combinations," *Proceedings of the 8th International Symposium on Ballistics,* Vol. IV, American Defense Preparedness Association, Arlington, VA, 1985, pp. 47-68.

[9]Nietubicz, C. J., and Sahu, J., "Navier-Stokes Computations of Base Bleed Projectiles," *Base Bleed: First International Symposium on Special Topics in Chemical Propulsion*, edited by K. K. Kuo and J. Fleming, Hemisphere, Washington, DC, 1991, pp. 93-106.

[10]Sahu, J., Nietubicz, C. J., and Steger, J. L., "Navier-Stokes Computations of Projectile Base Flow with and without Mass Injection," *AIAA Journal,* Vol. 23, No. 9, 1985, pp. 1348-1355.

[11]Nietubicz, C. J., Pulliam, T. H., and Steger, J. L., "Numerical Solution of the Azimuthal-Invariant Navier-Stokes Equations," U.S. Army Ballistic Research Lab., ARBRL-TR-02227, AD A085716, Aberdeen Proving Ground, MD, March 1980.

[12]Beam, R., and Warming, R. F., "An Implicit Factored Scheme for the Compressible Navier-Stokes Equations," AIAA Paper 77-645, June 1977.

[13]Sahu, J., and Nietubicz, C. J., "Improved Numerical Prediction of Transonic Flow," *Proceedings of the 4th Army Conference on Applied Mathematics and Computing,* U.S. Army Research Office, Durham, NC, May 1986, pp. 561-581.

[14]Sahu, J., Nietubicz, C. J., and Steger, J. L., "Navier-Stokes Computations of Projectiles Base Flow with and without Base Injection," U.S. Army Ballistic Research Lab., ARBRL-TR-02532, AD A135738, Aberdeen Proving Ground, MD, Nov. 1983.

[15]Baldwin, B. S., and Lomax, H., "Thin-Layer Approximation and Algebraic Model for Separated Turbulent Flows," AIAA Paper 78-257, Jan. 1978.

[16]Nietubicz, C. J., Heavey, K. R., and Steger, J. L., "Grid Generation Techniques for Projectile Configurations," *Proceedings of the 1982 Army Numerical Analysis and Computers Conference,* U.S. Army Research Office, Rept. 82-3, Durham, NC, Feb. 1982, pp. 99-121.

[17]Ding, Z., Liu, Y., and Chen, S., "A Study of Drag Reduction by Base Bleed at Subsonic Speeds," *Base Bleed: First International Symposium on Special Topics in Chemical Propulsion,* edited by K. K. Kuo and J. Fleming, Hemisphere, Washington, DC, 1991, pp. 241-250.

[18]Lieske, R. F., and Reiter, M. L., "Equations of Motion for a Modified Point Mass Trajectory," U.S. Army Ballistic Research Lab., BRL Rept. No. 1314, AD 485869, Aberdeen Proving Ground, MD, March 1966.

[19]Kayser, L. D., Kuzan, J. D., and Vazquez, D. N., "Flight Testing for 155MM Base Burn Projectile," U.S. Army Ballistic Research Lab., BRL-MR-3708, AD A201107, Aberdeen Proving Ground, MD, Nov. 1988.

[20]Lieske, R. F., "Determination of Aerodynamic Drag and Exterior Ballistic Trajectory Simulation for the 155mm, DPICM, M864 Base-Burn Projectile," U.S. Army Ballistic Research Lab., BRL-MR-3768, AD A209510, Aberdeen Proving Ground, MD, June 1989.

James E. Daywitt
Associate Editor